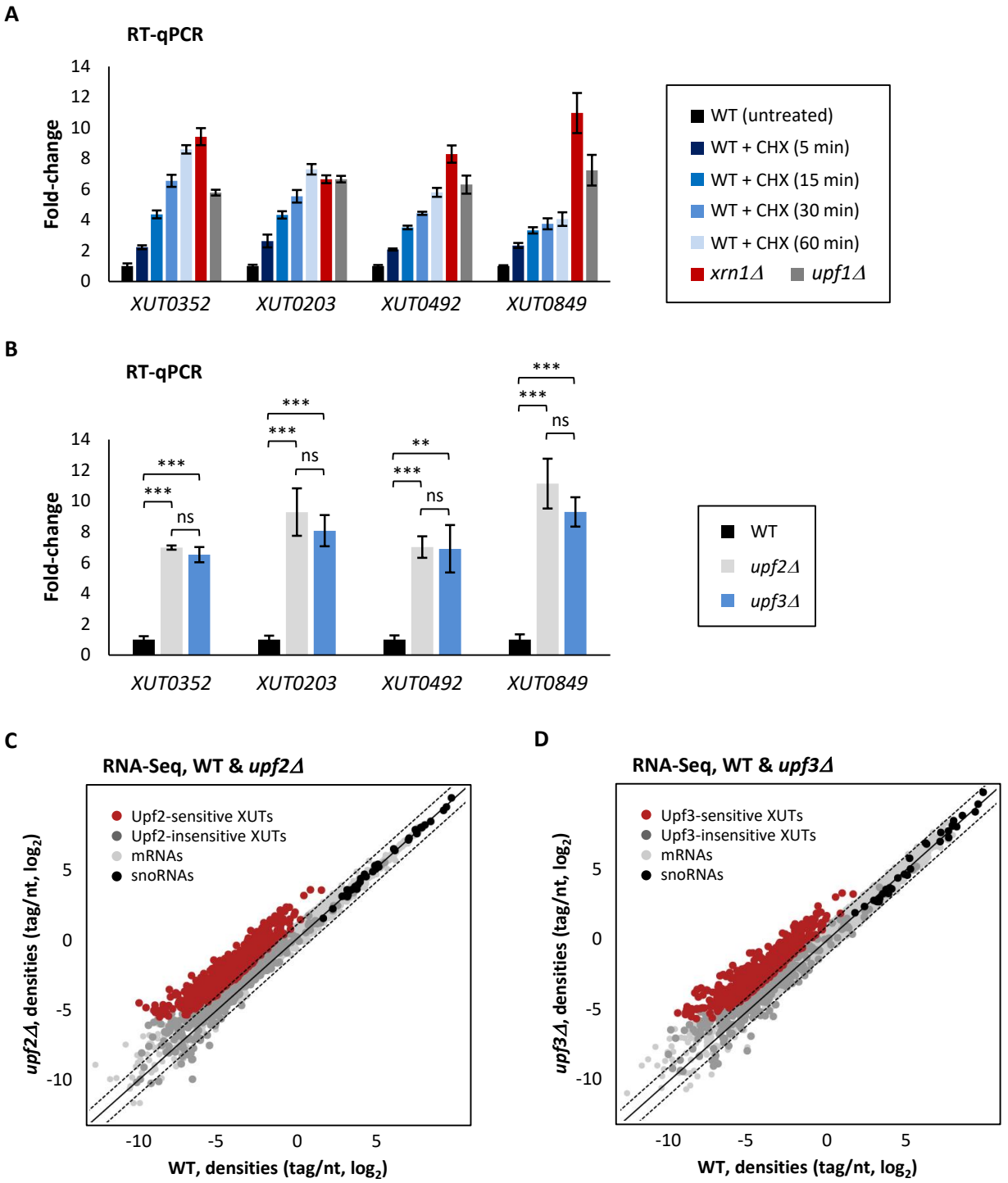

Figure S1. Sensitivity of XUTs to NMD and translation elongation inhibition.
(A) WT (YAM2478) cells were grown to mid-log phase. CHX was then added at a final concentration of 100 µg/mL, and samples were collected at different time points. Untreated *xrn1Δ* (YAM2479) and *upf1Δ* (YAM2890) cells were used as controls. After total RNA extraction, the levels of *XUT0352*, *XUT0203*, *XUT0492* and *XUT0849* were determined by strand-specific RT-qPCR, and normalized to *scR1*. The level of each XUT in untreated WT cells was set to 1. Mean and SD values were calculated from three independent biological replicates. **(B)** The levels of *XUT0352*, *XUT0203*, *XUT0492* and *XUT0849* were determined as above starting from total RNA extracted from exponentially growing WT (YAM2478), *upf2Δ* (YAM2967) and *upf3Δ* (YAM2968) cells. (***) *P*-value < 0.001; (**) *P*-value < 0.01; (ns) not significant upon *t*-test. **(C)** Scatter plot showing RNA-seq signals (tag densities, $\log_2$ scale) for Upf2-sensitive and Upf2-insensitive XUTs (red and dark grey dots, respectively), mRNAs (light grey dots), and snoRNAs (black dots) in WT and *upf2Δ* cells. The 520 Upf2-sensitive XUTs were defined using a fold change >2 and an adjusted *P*-value < 0.05 upon differential expression analysis using DESeq2 (see list in Table S1). **(D)** Same as above for Upf3-sensitive (n=542) and Upf3-insensitive XUTs, using RNA-Seq data obtained in WT and *upf3Δ* cells (see list in Table S1).

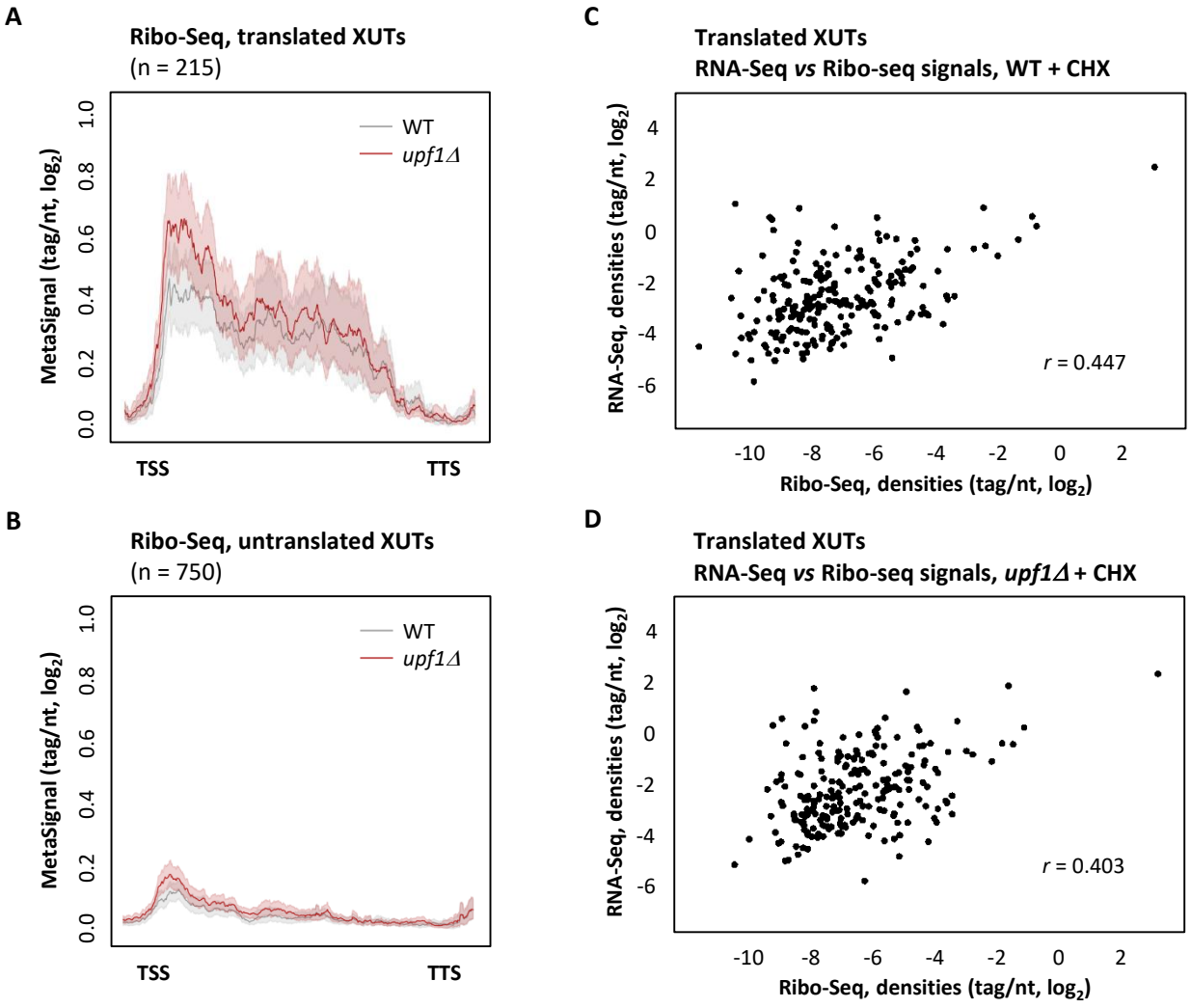

Figure S2. Translational landscape of XUTs in *N. castellii*.
(A) Metagene of Ribo-seq signals along the 215 translated XUTs in WT and *upf1Δ* cells. For each condition, densities (tag/nt, $\log_2$) along the XUTs ±100 nt were piled up, then the average signal was plotted. The shading surrounding each line denotes the 95% confidence interval. **(B)** Same as above for the 750 XUTs that were defined as untranslated. **(C)** Scatter plot showing the Ribo-seq and RNA-seq signals (tag/nt, $\log_2$ scale) for the translated XUTs in CHX-treated WT cells. The Pearson correlation coefficient (*r*) is indicated. **(D)** Same as above in CHX-treated *upf1Δ* cells.

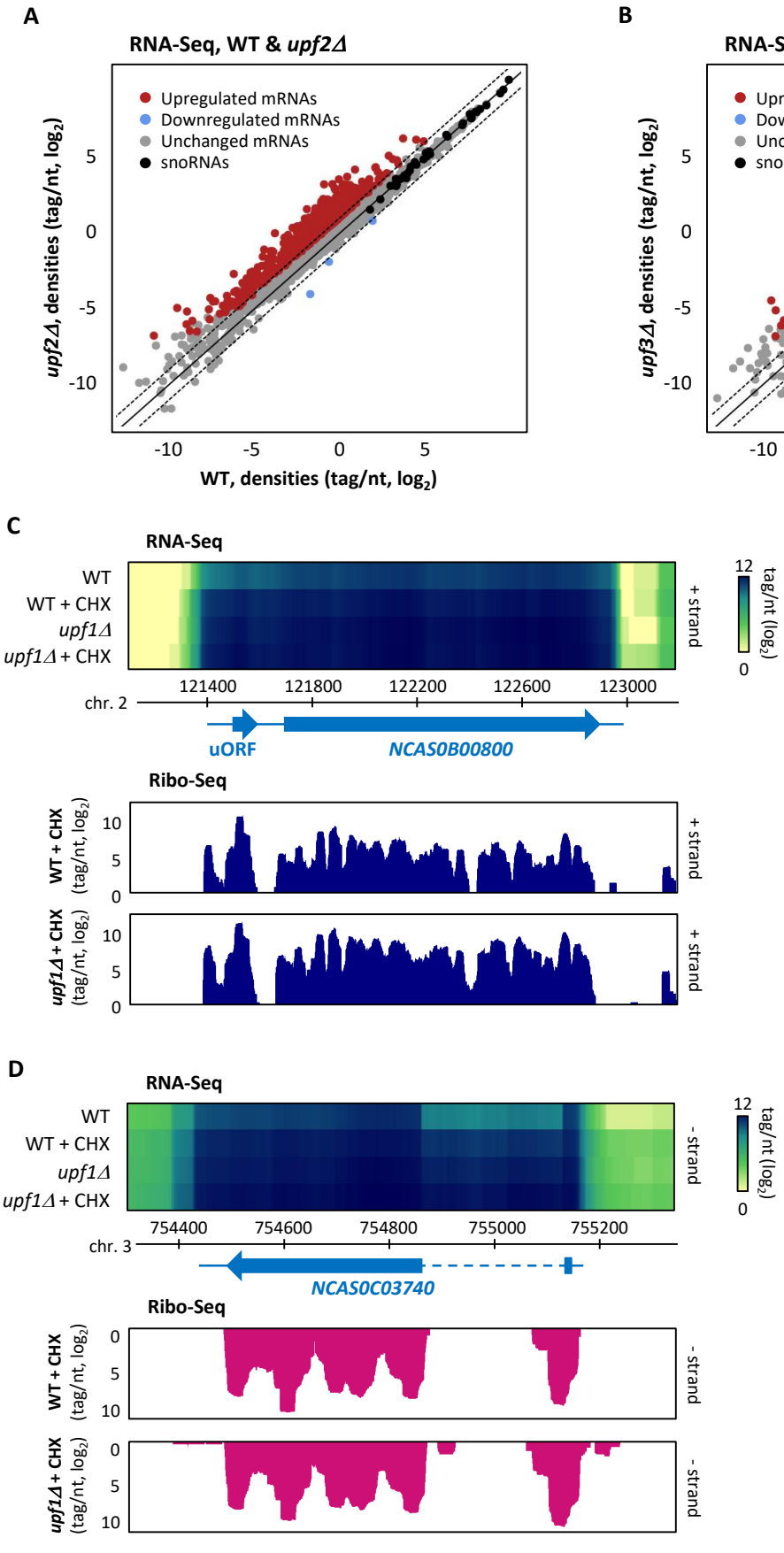

Figure S3. NMD-sensitive mRNAs of *N. castellii*.
(A) Total RNA-seq was performed using total RNA extracted from exponentially growing WT and *upf2Δ* cells. The scatter plot shows the RNA-seq signals (tag densities, $\log_2$ scale) for upregulated mRNAs (NMD-sensitive; red), downregulated mRNAs (blue), unaffected mRNAs (grey) and snoRNAs (black). **(B)** Same as above using total RNA extracted from exponentially growing WT and *upf3Δ* cells. **(C)** Snapshot of RNA-seq (upper panel) and Ribo-seq (lower panels) signals across the *CPA1* (*NCAS0B00800*) mRNA, produced using the VING software (Descrimes *et al.*, 2015). The blue line and the long arrow represent the mRNA and the canonical ORF. The small arrow represents the uORF in the 5' UTR of the *CPA1* mRNA. **(D)** Same as above for the *RPL22B* (*NCAS0C03740*) mRNA. The dashed blue line represents the intron.

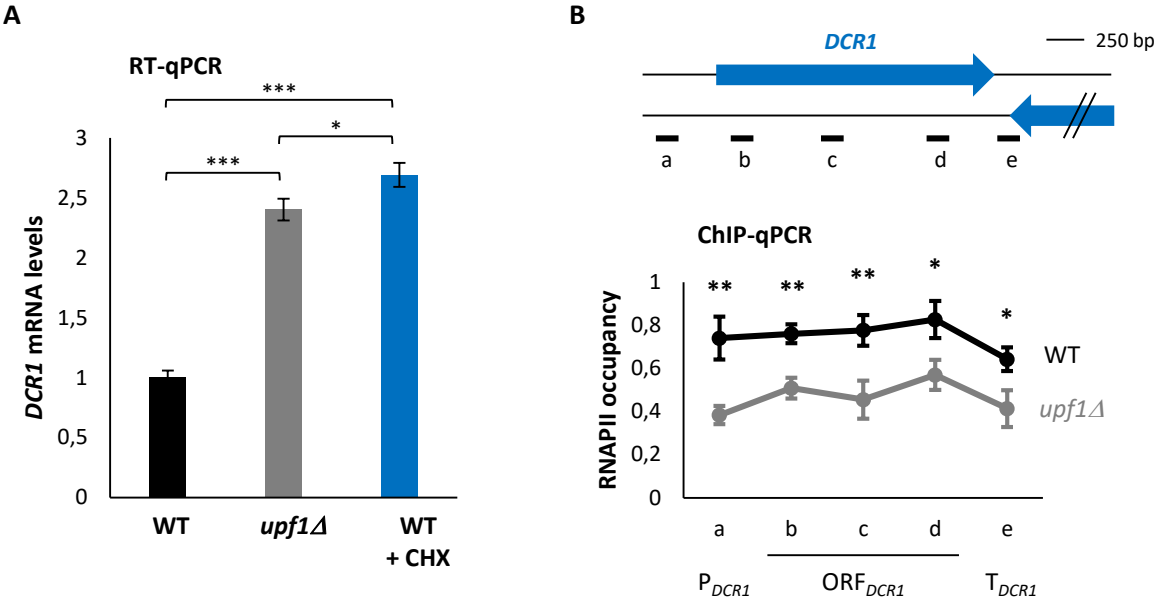

Figure S4. *DCR1* is regulated by NMD.

(A) The levels of *DCR1* mRNA were determined as described in Supplemental Fig. 1A, in untreated WT and *upf1Δ* cells, and in CHX-treated WT (15 min of treatment with 100 µg/mL CHX). (***) *P*-value < 0.001; (*) *P*-value < 0.05 upon *t*-test.

(B) *Upper panel*. Schematic representation of the *DCR1* locus indicating the position of the different probes used for the ChIP analysis (see Table S4 for sequences). *Lower panel*. RNAPII occupancy across the *DCR1* locus was determined by ChIP in WT and *upf1Δ* cells. Positions a, b-d and e correspond to the promoter, coding and terminator regions of *DCR1*, respectively. Data (IP/input) for each position were normalized to the values obtained for the *RPO21* gene body, used as a reference since it is not regulated by NMD (see Table S2). Mean and SD values were calculated from three independent biological replicates. (**) *P*-value < 0.01; (*) *P*-value < 0.05 upon *t*-test.

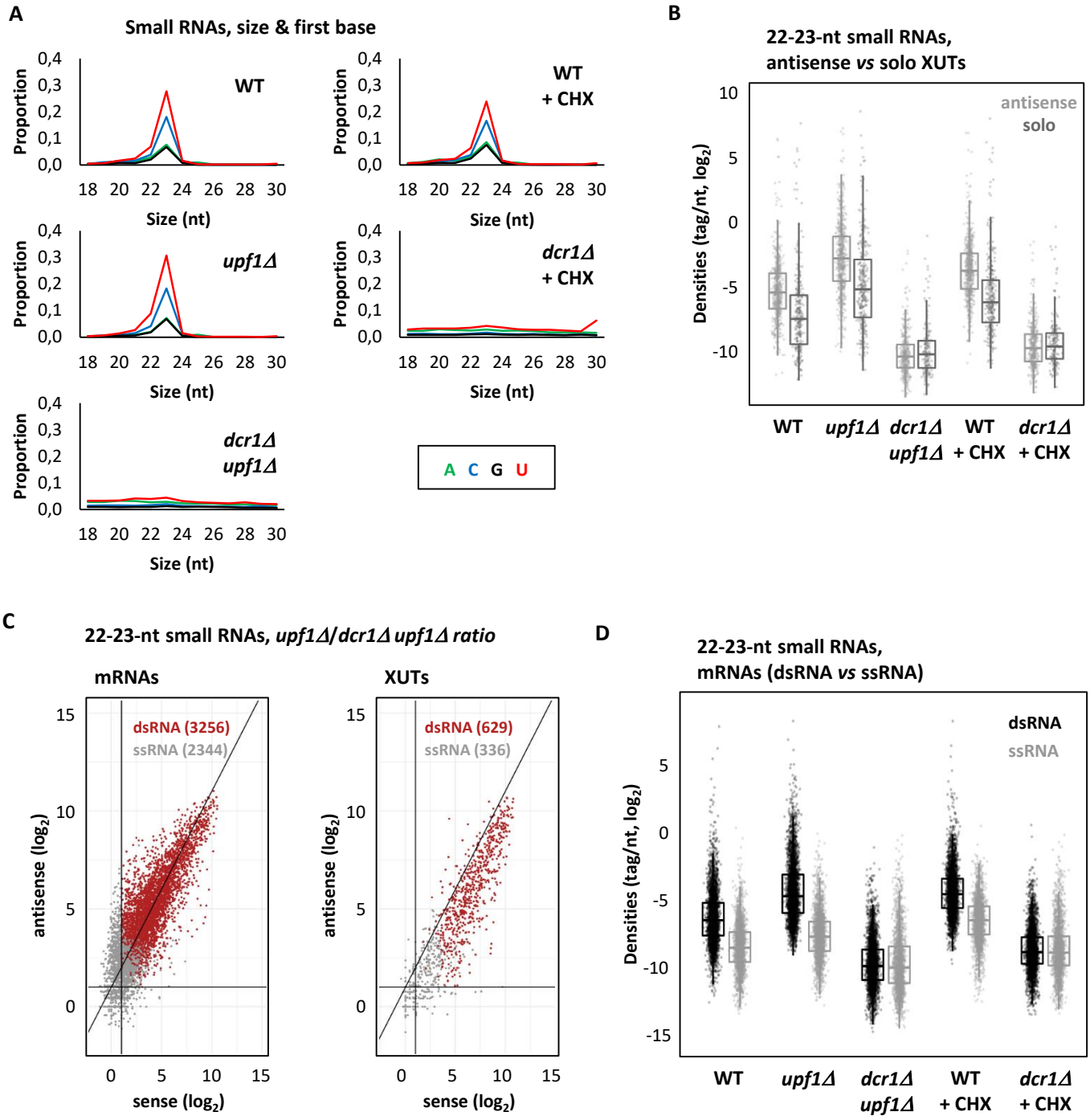

Figure S5. Antisense NMD-sensitive XUTs are preferentially processed by Dcr1 into small RNAs.
(A) Size and first base of uniquely mapped small RNA reads in untreated and CHX-treated WT (YAM2478), *upf1Δ* (YAM2890), *dcr1Δ upf1Δ* (YAM2943), and CHX-treated *dcr1Δ* (YAM2795) cells. **(B)** Densities of 22-23-nt small RNAs (tag/nt, $\log_2$ scale) for the antisense (light grey) and solo (dark grey) XUTs in WT, *upf1Δ*, *dcr1Δ upf1Δ*, CHX-treated WT and CHX-treated *dcr1Δ* cells. **(C)** Identification of dsRNA-forming mRNAs and XUTs. The data are presented as ratios ($\log_2$ scale) of 22-23-nt small RNA signals in the *upf1Δ* strain over the *dcr1Δ upf1Δ* strain, for the sense (*x*-axis) and antisense (*y*-axis) strands, including a threshold at least 10 reads per transcript. The 3256 mRNAs and 629 XUTs found to form dsRNA are highlighted as red dots, in the left and right panels, respectively. The transcripts defined as single-stranded (ssRNA) are represented as grey dots. **(D)** Densities of 22–23-nt small RNAs (tag/nt, $\log_2$ scale) for dsRNA-forming (black) and single-strand (ssRNA; grey) mRNAs in WT, *upf1Δ*, *dcr1Δ upf1Δ*, CHX-treated WT and CHX-treated *dcr1Δ* cells.

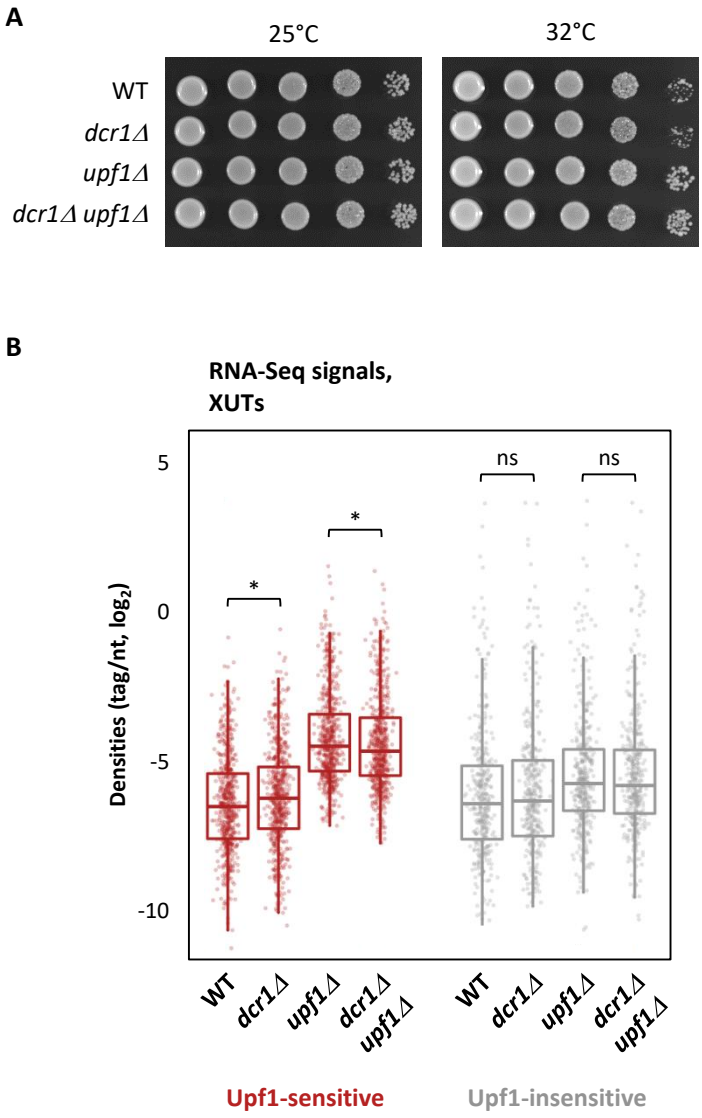

Figure S6. Inactivation of Dcr1 reduces RNA accumulation in Upf1-deficient cells.
(A) Serial dilutions of WT (YAM2478), *dcr1Δ* (YAM2795), *upf1Δ* (YAM2890) and *dcr1Δ upf1Δ* (YAM2943) cells were dropped on rich medium (YPD), and then incubated at the indicated temperatures for 2 days. **(B)** Total RNA-seq was performed using total RNA extracted from exponentially growing WT, *dcr1Δ*, *upf1Δ* and *dcr1Δ upf1Δ* cells. Data are presented as densities (tag/nt, $\log_2$ scale) for the Upf1-sensitive and Upf1-insensitive XUTs in each strain. (*) *P*-value < 0.05; (ns) not significant upon Wilcoxon rank-sum test (adjusted for multiple testing with the Benjamini–Hochberg procedure).

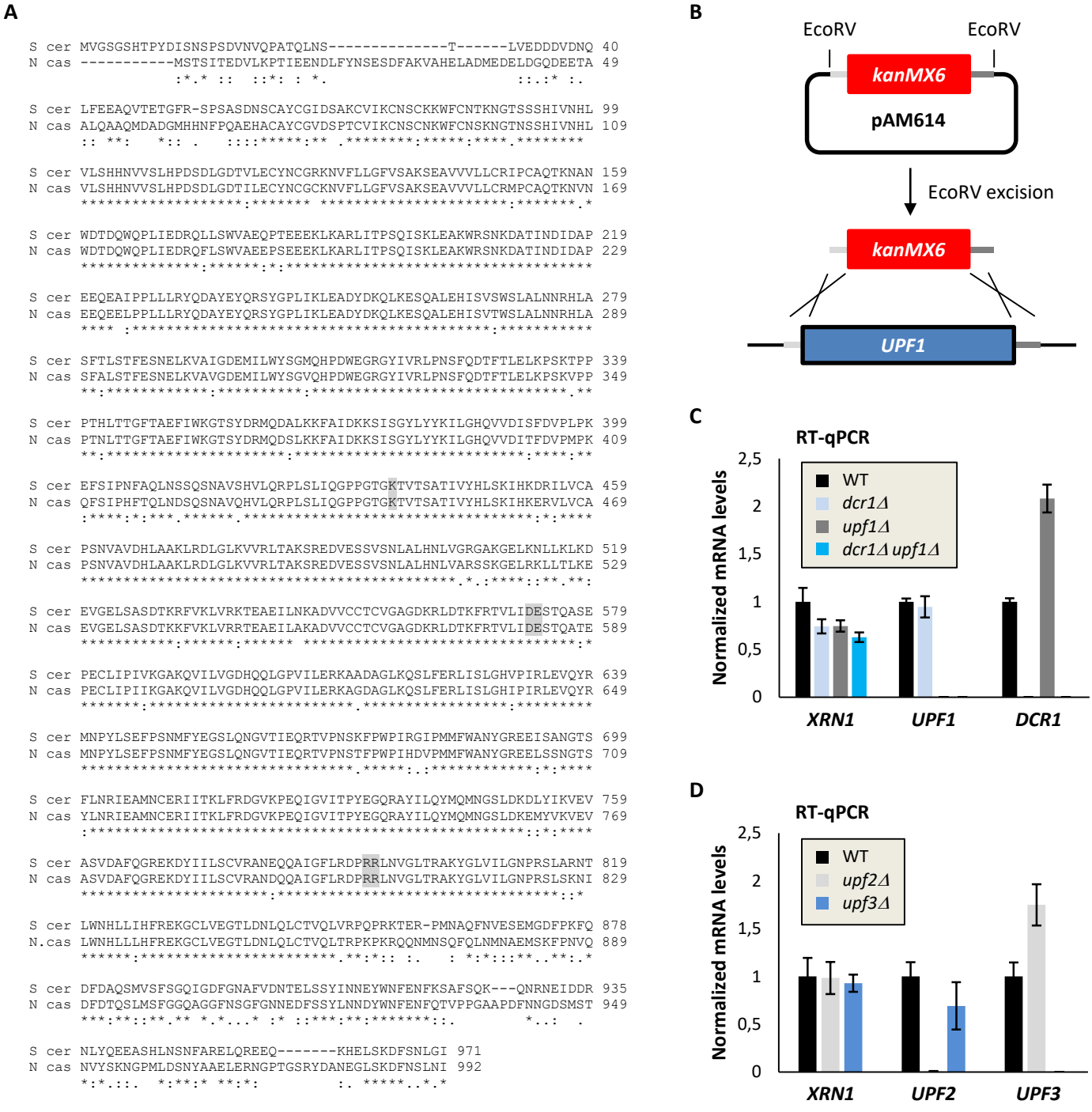

Figure S7. Identification and deletion of NMD core factors in *N. castellii*.

(A) Alignment of Upf1 protein sequence from *S. cerevisiae* (*YMR080C* gene product) and *N. castellii* (*NCAS0A07730* gene product). Sequences were aligned using CLUSTAL O (version 1.2.4). Key: asterix (*) for fully conserved residue, colon (:) for amino acid groups of similar properties, period (.) for amino acid groups of weakly similar properties. Critical residues for ATP binding (K436 in *S. cerevisiae*), ATP hydrolysis (D572 & E573 in *S. cerevisiae*) and RNA binding (R793 & R794 in *S. cerevisiae*) are highlighted. **(B)** Overview of the strategy to delete *UPF1* in *N. castellii* by homologous recombination using a *kanMX6* marker flanked by long *UPF1* targeting sequences. The light and dark grey boxes represent the 287 bp and 436 bp that precede and follow the *UPF1* ORF, respectively. The deletion cassette can be excised by EcoRV digestion. **(C)** Validation of the YAM2478 (WT), YAM2795 (*dcr1Δ*), YAM2890 (*upf1Δ*) and YAM2943 (*dcr1Δ upf1Δ*) strains. After total RNA extraction, levels of *XRN1*, *UPF1* and *DCR1* mRNAs were assessed by strand-specific RT-qPCR, and normalized to *scR1*. The level of each mRNA in the WT strain was set to 1. Mean and SD values were calculated from three independent biological replicates. **(D)** Validation of the YAM2967 (*upf2Δ*) and YAM2968 (*upf3Δ*) strains. *XRN1*, *UPF2* and *UPF3* mRNA levels were assessed as above.